Journal of Applied Electrochemistry (2006) 36:115–130
DOI 10.1007/s10800-005-9044-4

Mathematical model for a direct propane phosphoric acid fuel cell

G. PSOFOGIANNAKIS[1,4], Y. BOURGAULT[2], B. E. CONWAY[3,4] and M. TERNAN[4,5,*]
[1]*Department of Chemical Engineering, The University of Ottawa, Ottawa, Ont., K1N 6N5, Canada*
[2]*Department of Mathematics and Statistics, The University of Ottawa, Ottawa, Ont., K1N 6N5, Canada*
[3]*Department of Chemistry, The University of Ottawa, Ottawa, Ont., K1N 6N5, Canada*
[4]*Centre for Catalysis Research and Innovation, The University of Ottawa, Ottawa, Ont., K1N 6N5, Canada*
[5]*EnPross Inc., 147 Banning Road, Ottawa, Ont., K2L 1C5, Canada*
*(*author for correspondence, e-mail: ternan@sympatico.ca)*

Received 21 October 2004; accepted in revised form 27 July 2005

Key words: electrochemical oxidation, fuel-cell, hydrocarbon, hydrocarbon oxidation, modeling, PAFC, phosphoric acid, propane

Abstract

A mathematical model was developed and used to predict the performance of direct propane phosphoric acid (PPAFC) fuel cells, utilizing both Pt/C state-of the-art electrodes and older Pt black electrodes. It was found that the overpotential caused by surface processes on the platinum catalyst in the anode is much greater than the potential losses caused by either ohmic resistance or propane diffusion in gas-filled and liquid-filled pores. In one comparison, the anode overpotential (0.5 V) was larger than the cathode overpotential (0.3 V) at a current density of 0.4 A cm^{-2} for Pt loadings 4 mg Pt cm^{-2}. The need for sufficient water concentration at the anode, where water is a reactant, was indicated by the large effect of H_3PO_4 concentration. In another comparison, the model predicted that at 0.2 A cm^{-2}, modern carbon supported Pt catalysts would produce 0.35 V compared to 0.1 V for unsupported Pt black catalysts that were used several decades ago, when the majority of the research on direct hydrocarbon fuel cells was performed. The propane anode and oxygen cathode catalyst layers were modeled as agglomerates of spherical catalyst particles having their interior spaces filled with liquid electrolyte and being surrounded by gas-filled pores. The Tafel equation was used to describe the electrochemical reactions. The model incorporated gas and liquid-phase diffusion equations for the reactants in the anode and cathode and ionic transport in the electrolyte. Experimental data were used for propane and oxygen diffusivities, and for their solubilities in the electrolyte. The accuracy of the predicted electrical potentials and polarization curves were normally within ± 0.02 V of values reported in experimental investigations of temperature and electrolyte concentration. Polarization curves were predicted as a function of temperature, pressure, electrolyte concentration, and Pt loading. A performance of 0.45 V at 0.5 A cm^{-2} was predicted at some conditions.

List of symbols

a: anodic transfer coefficient for propane oxidation or cathodic transfer coefficient for oxygen reduction
a_A: anodic transfer coefficient for the propane oxidation reaction
a_C: cathodic transfer coefficient for the oxygen reduction reaction
a_W: activity of water in the electrolyte
c^*: solubility of propane or oxygen in H_3PO_4 (mol cm^{-3} Pa^{-1})
c_P^{**}: solubility of propane in H_3PO_4 at 101.3 kPa reactant partial pressure (mol cm^{-3})
c^G: concentration of reactant in the gas phase (mol cm^{-3})
c_P^G, c_P: concentration of propane in the gas phase (mol cm^{-3})
c_P^D: concentration of propane dissolved in the electrolyte (mol cm^{-3})
c_W: concentration of water vapor in the gas phase (mol cm^{-3})
c_{CO_2}: concentration of carbon dioxide in the gas phase (mol cm^{-3})
c_T: total gas concentration (mol cm^{-3})
D: diffusivity of propane or oxygen in the electrolyte (cm^2 s^{-1})
D^E: effective diffusivity of reactant gas within agglomerates (cm^2 s^{-1})
$D_{P/W}^E$: effective binary diffusion coefficient for propane and water vapor (cm^2 s^{-1})
D_{P/CO_2}^E: effective binary diffusion coefficient between propane and carbon dioxide (cm^2 s^{-1})
E_{EQ}: equilibrium potential (V)
E_{CELL}: cell potential (V)

E_{CAT}: cathode potential (V)
E_{AN}: anode potential (V)
F: Faraday constant, (96487 C mol^{-1})
iR: (Eq 23) electrical potential loss in the electrolyte layer (V)
j: cell current density (A cm^{-2})
j_o: exchange current density on platinum (A [cm^2 Pt]$^{-1}$)
j_o^*: reference exchange current density (A [cm^2 Pt]$^{-1}$)
j_+: net ionic current density (A cm^{-2})
K: Henry's law constant for oxygen or propane in phosphoric acid
k_E: effective specific conductivity of electrolyte in catalyst layer (S cm^{-1})
L_{CL}: thickness of catalyst layer (cm)
L_{ELL}: thickness of the electrolyte layer (cm)
L_F: thickness of liquid film (cm)
M_{Pt}: platinum loading per unit electrode surface area (g Pt [cm^2 electrode]$^{-1}$)
m: molality of the electrolyte solution (mol H_3PO_4 [kg H_2O]$^{-1}$)
n: number of moles of electrons transferred per mole of reactant consumed
N_P: propane molar flux (mol cm^{-2} s^{-1})
N_{CO_2}: carbon dioxide molar flux (mol cm^{-2} s^{-1})
R: ideal gas constant 8.3145 J mol^{-1} K^{-1}
r_{AG}: the agglomerates radii (cm)
R_V: volumetric reaction rate in the catalyst layer [moles reactant consumed per unit volume catalyst layer per unit time] (mol cm^{-3} s^{-1})
S_{Pt}: the surface area per unit mass of platinum that is available for reaction (cm^2 Pt [g Pt]$^{-1}$)
S_A: surface area of platinum per unit volume in agglomerate (cm^2 Pt [cm^3 agglomerate]$^{-1}$)
T: temperature (K)
T^*: reference temperature for the exchange current density (K)
V: (Equation 20) molar volume (cm^3 mol^{-1})
W: the nominal weight percentage of phosphoric acid solution (100*g H_3PO_4 [g $H_3PO_4 + H_2O$]$^{-1}$)
$W_{F/Pt}$: weight fraction of platinum in catalyst (mass of Pt [mass of Pt + C]$^{-1}$)
x: (Equation 5) reaction order with respect to water activity
η: local overpotential (V)
$\Delta G^{\ddagger}$: activation energy for the exchange current density (J mol^{-1})
z: coordinate along catalyst layer or gas diffusion layer (increasing towards the electrolyte layer)
ρ_{uAG}: utilized agglomerates' density (number of utilized agglomerates per unit volume catalyst layer)
Φ_L: electrical potential in the liquid electrolyte (V)
Φ_S: electrical potential in the solid (V)
ψ: parameter defined in Equation 6

1. Introduction

This work describes a mathematical model of a direct hydrocarbon fuel cell (DHFC) operating at moderate-temperatures ($T < 250$ °C). In a DHFC a gaseous or liquid hydrocarbon fuel is directly oxidized at the anode of the fuel cell without first being converted into another fuel, such as hydrogen, prior to the electrochemical reaction. Although DHFCs have been greatly overshadowed by hydrogen and methanol fuel cells a substantial amount of research on the electrochemical oxidation of hydrocarbons was published during the period from 1959 to 1968. Comprehensive reviews have been published by Liebhafsky and Cairns [1], Bockris and Srinivasan [2] and Cairns [3]. Some of that work is highlighted briefly here.

The acid–base characteristics of the electrolyte have a major influence on the performance of DHFCs. Basic electrolytes such as KOH react with the CO_2 that results from the oxidation of hydrocarbons and thereby cause K_2CO_3 to precipitate. This was avoided by using Rb_2CO_3–$RbHCO_3$ and Cs_2CO_3–$CsHCO_3$ electrolytes [4]. Nevertheless, the best aqueous electrolytes (both chemically inert and not adsorbed on the platinum electrode) for DHFCs are strong acids with high temperature boiling points [1, 3]. A comparison of several acids at the same conditions [5] found that the best performance was obtained with an aqueous HF electrolyte. Unfortunately HF–H_2O mixtures form an azeotrope with a maximum boiling point of 120 °C compared to a 200 °C boiling point for aqueous H_3PO_4 mixtures. The increase in operating temperature that is possible with H_3PO_4 fuel cells increases kinetics and current densities. A binary CsF–HF electrolyte that operated at elevated temperatures was also promising but it had water management problems [6]. Therefore, H_3PO_4 was considered to be the most practical electrolyte [1] and was chosen as the electrolyte for this study. Furthermore, the commercial scale operation of hydrogen phosphoric acid fuel cells (PAFC) confirms H_3PO_4 as a practical electrolyte.

At certain conditions DHFCs exhibit a cycling phenomenon that has been attributed to carbonaceous oligomers and electrolyte anions that may be adsorbed on the anode [3]. During each cycle, the adsorbed species block reaction sites on the electrode, decrease the useful electrode surface area, and thereby decrease the rate of the electrode reaction. Eventually the electrode potential attains a value that is sufficient to oxidize and remove the oligomers. With H_3PO_4 electrolyte, cycling is absent when the fuel is methane and is tolerable when it is propane [1].

Several other factors influence the performance of DHFCs. An investigation of various fuels [6], concluded that the largest oxidation rates were obtained with propane. In sufficiently concentrated electrolytes, the small water content may cause the rate of water diffusion to be rate-limiting [3]. Hydrocarbon solubility in electrolytes as well as both adsorption and reaction on metal catalysts have also been reviewed [2]. It was reported [3] that the performance of platinum was superior to the other catalysts, and that an activation energy of 58–84 kJ mol^{-1} was obtained for the overall rate of hydrocarbon oxidation in acid electrolytes. The choice of the catalyst is virtually limited to platinum or platinum alloys because the hot acidic environment of the electrolyte is corrosive [1].

Various mechanisms for the hydrocarbon reaction at the anode of a DHFC have been suggested. It was proposed [7] that the hydrocarbon is dissociatively chemisorbed to form an adsorbed hydrogen atom and a carbonaceous species that subsequently dehydrogenates forming additional hydrogen atoms and other surface species that ultimately either convert to CO_2 or oligomerize to form a carbonaceous residue on the electrode surface. An alternative mechanism [8] suggested that the rate determining step was the chemical reaction between an adsorbed hydrocarbon (acetylene) and an adsorbed OH species that resulted from water dissociation. Later [9] it was suggested that alkanes react by dissociative chemisorption followed by surface dissociation to form lower molecular weight species. Results with methane [10] were explained by (a) dissociative chemisorption, (b) partial oxidation of the adsorbed species and (c) reaction with an adsorbed OH species to form CO_2.

Only a few investigations on DHFCs have been performed since 1968. The kinetic parameters for the ethylene reaction on gold electrodes have been determined [8, 11]. It was proposed [12] that CH_4 chemisorbs dissociatively to CH_3(ads), H^+, and e^- followed by the rate determining step through which CH_3(ads) formed intermediates. Bagotzky et al. [13] proposed a mechanism in which a chemisorbed hydrocarbon reacts in combinations of (a) dehydrogenation reactions and (b) reactions with adsorbed hydroxyl groups. Electroadsorption studies of methane have been explained using the Bagotzky mechanism [14]. *In situ* infrared spectroscopy experiments [15] on electrodes immersed in $HClO_4$ electrolyte, identified the following species, H —C* =O, HO —C* =O, and =C =O. No evidence for CH_X species was found. An investigation of DHFCs using Nafion and polybenzimidazole membranes [16] obtained performances at 95 °C that were comparable to those in aqueous H_3PO_4 at 175 °C [17].

Propane was the hydrocarbon chosen in this study for three reasons. First, it is used as a heating fuel that is commonly available in rural areas, so that both delivery and storage infrastructure already exist. The cost of supplying conventional electricity in rural areas is much greater than in urban areas. Consequently fuel cells are likely to become cost competitive with electricity from the grid for niche applications such as this, prior to their use in large volume applications such as the automotive market. Second, the performance of propane fuel in direct hydrocarbon fuel cells has been found to be slightly better than other low molecular weight alkanes. A third reason is that experimental data for well-characterized PPAFCs with propane as fuel were found in the literature for several operating conditions so that the results of this model could be compared to experiment.

The structure of gas diffusion electrodes used in hydrogen phosphoric acid fuel cells (PAFC's) has improved since the time that most of the performance data on DHFCs in aqueous electrolytes were obtained. Current hydrogen fuel cell catalysts using platinum dispersed on carbon [18] have amounts of platinum surface area per unit mass of catalyst m^2 $(g\ Pt)^{-1}$ that are nearly 10-fold greater than those in the older DHFCs reported for platinum black electrodes [19]. Modern gas diffusion and catalyst layers have been designed to improve gas permeability and wettability by a liquid electrolyte. Furthermore, the thickness of the electrolyte compartment between the electrodes has been decreased to nearly 1/10th of the previous thickness by utilizing silicon carbide matrices. The smaller ohmic losses also improve the DHFC's performance.

The present work describes what we believe is the first application of mathematical modeling techniques for predicting the performance of any moderate temperature (100–250 °C) direct hydrocarbon fuel cell. This study used propane as the fuel and phosphoric acid as the electrolyte. The model was used: (1) to simulate experimental results that have been published in the literature, (2) to predict the performance of DHFCs with state-of-the-art PAFC electrodes, (3) to describe the influence of operating variables (temperature, gas pressure, acid concentration) and electrode design parameters (catalyst loading, electrode thickness, fraction of Pt in Pt/C catalyst) and (4) to determine the electrical potential losses that are caused by electrocatalyst surface processes, gas diffusion, and ionic transport.

2. Mathematical model description

The model presented here for a DHFC describes a propane anode, a phosphoric acid electrolyte and an air (or oxygen) cathode. Our numerical simulation of the cathode electrode and phosphoric acid electrolyte is conceptually similar to those of hydrogen fuel cells [20] and has already been validated [21] against experimental half-cell cathode data. Since there is a reasonable degree of confidence in our simulation of the cathode and electrolyte, a favorable comparison of our DHFC model with data for DHFC's should validate our description of the anode.

In a direct propane fuel cell with aqueous electrolyte, the overall reaction is:

$$C_3H_8 + 5\ O_2 \rightarrow 3\ CO_2 + 4\ H_2O \quad (1)$$

The reaction on the anode catalyst surface is:

$$C_3H_8 + 6\ H_2O \rightarrow 3CO_2 + 20\ H^+ + 20\ e^- \quad (2)$$

The reaction on the cathode catalyst surface is:

$$5O_2 + 20\ H^+ + 20\ e^- \rightarrow 10\ H_2O \quad (3)$$

A steady-state, isothermal model was developed for the direction normal to the fuel cell external surface, through the various fuel cell layers; a gas channel (GC), a gas diffusion layer (GDL), and a catalyst layer (CL) for both the anode and the cathode, as well as an electrolyte layer (ELL). It also describes the physicochemical phenomena that occur in those layers: gas diffusion in gas-filled pores, gas dissolution, dissolved gas diffusion in liquid-filled pores, ohmic conduction, and electrochemical reaction. We used a variation of the standard flooded agglomerate model [20–30] that has successfully described the diffusion, adsorption, and reaction phenomena in cathode and anode electrodes of hydrogen phosphoric acid fuel cells (PAFC) and polymer electrolyte fuel cells (PEMFC). The agglomerate model describes the electrode's catalyst layer as a collection of homogeneously distributed spherical agglomerates that are composed of carbon particles on which the electrocatalyst platinum particles are dispersed. The spaces between the agglomerates form pores that are flooded with H_3PO_4 electrolyte. The flooded agglomerates are surrounded by a thin liquid electrolyte film. Polytetrafluoroethylene (PTFE) particles are on the exterior of the C/Pt agglomerates. They are hydrophobic so that the spaces between the agglomerates and the PTFE particles consist of gas-filled pores used for transport of reactant and product gases through the electrode catalyst layer.

The reactants, oxygen gas at the cathode and propane gas at the anode, are transported by molecular diffusion from the gas channels through the gas diffusion layer and then through the gas-filled macropores of the catalyst layer. The reactant gases dissolve in the electrolyte at the outer surface of the liquid film surrounding the agglomerates, diffuse through the liquid film, diffuse through the liquid filled pores within the agglomerate, and react electrochemically on the platinum surface. The product carbon dioxide in the anode follows the reverse route. The water vapor pressure inside the electrode pores is the equilibrium vapor pressure at the specified temperature and concentration of H_3PO_4 electrolyte. Ionic transport occurs in the liquid within the catalyst layers and in the electrolyte layer. The electrical potential gradient required for ionic conductivity in the electrolyte in the catalyst layers and the gas (oxygen, carbon dioxide, and propane) concentration distributions within the catalyst layer affect the electrode potential and current density distributions throughout the catalyst layer. Most of the equations shown below are for the propane anode. Analogous equations have been used for the cathode.

The electrochemical reactions were described using the Tafel equation. For both the oxygen reduction reaction and the propane oxidation reaction, the reaction rates have been reported [2, 31] to exhibit first order dependence on the concentration of dissolved reactant. In addition, it was assumed that the propane oxidation reaction exhibits first-order dependence on the activity of water in the phosphoric acid solution, because water is also a reactant in the anodic reaction. For the propane oxidation reaction at the anode, the Tafel equation is:

$$j = j_o\left(\frac{c_P^D a_W}{c_P^{**}}\right)\left[\exp\left(\frac{a_A nF\eta}{RT}\right)\right] \quad (4)$$

An equation similar to Equation 4 can be written for the cathode reaction in which the exponential term has a negative sign, and the symbols for quantities at the propane anode are replaced by their analogs at the oxygen cathode.

The reaction rate equations were derived by considering equations for simultaneous radial diffusion and reaction in the agglomerates, as well as radial-diffusion equations for the liquid film surrounding the agglomerates. Derivation of the equations [21] for the reaction rate requires satisfying the boundary conditions of (a) zero net reactant flux at the center of the agglomerate, (b) equal reactant concentration at the two sides of the boundary between the agglomerate and the liquid film, and (c) Henry's law relationship between the dissolved gas concentration of the reactant at the outside surface of the liquid film and the reactant partial pressure in the gas-filled pores. Moreover, different effective reactant diffusivities are used for the liquid film and the agglomerate, since only the latter requires correction for porosity and tortuosity. Our equations differ from those used previously [20] in that the present equations include a liquid film with the geometry of a spherical shell. The following equation, for either the cathode or the anode, was derived for the volumetric reaction rate per unit volume of catalyst layer, where the variables refer to the respective reactant, reaction, or electrode:

$$R_V = \rho_{uAG} \times \frac{4\pi D^E D(r_{AG}+L_F)Kc^G a_w^x r_{AG}[r\sqrt{\psi}\coth(r_{AG}\sqrt{\psi})-1]}{D(r_{AG}+L_F)+L_F D^E[r_{AG}\sqrt{\psi}\coth(r_{AG}\sqrt{\psi})-1]} \quad (5)$$

The exponent x on the water activity a_w was taken as unity for propane oxidation, where water is a reactant, and zero for oxygen reduction, where water is a reaction product. The parameter ψ [21] is given by

$$\psi = \left(\frac{S_A j_o}{z^E F c^{**} D^E}\right)\left[\exp\left(\frac{\alpha nF\eta}{RT}\right)\right] \quad (6)$$

where α is either the anodic transfer coefficient for propane oxidation, a_A, or the cathodic transfer coefficient for oxygen reduction, a_C, depending on the

electrode for which the equation is applied. Equation 6 is valid for the anode. For the cathode, the exponential term will have a negative sign. S_A is related to the surface area per unit mass of platinum S_{Pt} through the following relationship:

$$S_A = \frac{(M_{Pt})(S_{Pt})}{(L_{CL})(V_{FAG})} \quad (7)$$

The platinum surface area S_{Pt} [cm^2 Pt (g Pt)$^{-1}$] is a function of the catalyst composition $W_{F/Pt}$ [g Pt (g Pt + C)$^{-1}$]. As the Pt content of the catalyst increases, the size of the platinum crystallites increases and this causes the effective surface area of platinum to decrease. A correlation [21] based on commercial catalyst data (from E-TEK) was used to describe this effect. All the correlations (including exponential and polynomial correlations) used in this study were obtained by linear least squares fitting.

$$S_{Pt} = 10^4(131 W_{F/Pt}^2 - 302.2 W_{F/Pt} + 168.3) \quad (8)$$

Values for the electrochemical parameters, j_0, a_A, and a_C, in Equation 4 and 6 were taken from the literature. For the oxygen reduction reaction on Pt metal in concentrated acid electrolyte, at conditions sufficiently far away from equilibrium, the cathodic transfer coefficient was reported [25] to be $\alpha_C = 1$, while for propane oxidation the anodic transfer coefficient was reported [2] to be $\alpha_A = 1$. The values used here, in combination with the exchange current densities determined from experimental Tafel plots, result in a phenomenological description of the reaction rate that is consistent with experimental data. An Arrhenius-type expression was used to account for the variation in exchange current density with temperature:

$$j_o = j_o^* \exp\left[(\Delta G^{\ddagger}/R)\left(\frac{1}{T^*} - \frac{1}{T}\right)\right] \quad (9)$$

The exchange current density for oxygen reduction on platinum in phosphoric acid was calculated [32] from experimental Tafel slopes to be $j_o^* = 3.8 \times 10^{-13}$ A (cm^2 Pt)$^{-1}$ at $T^* = 298$ K, and the activation energy for the exchange current density for oxygen reduction on Pt was reported to be $\Delta G^{\ddagger} = 92$ kJ mol^{-1} [32, 33]. For propane oxidation on platinum catalyst in acid electrolyte, the following values were found to be consistent with experimental data[17]: $j_o^* = 10^{-8}$ A (cm^2 Pt)$^{-1}$ at $T^* = 150$ °C and $\Delta G^{\ddagger} = 90$ kJ mol^{-1} for the temperature range 120–250 °C. The model electrochemical parameters are summarized in Table 1.

The overpotential at any position in the catalyst layer of each electrode is given by

$$\eta = \phi_S - \phi_L - E_{EQ} \quad (10)$$

where the overpotential η is positive for the anode and negative for the cathode. The electrical potential in the electrolyte within the catalyst layer, ϕ_L, varies with the thickness of the catalyst layer. An electrical potential gradient in the electrolyte is required for ionic conduction and is determined by the rate of proton production (anode) or consumption (cathode) and therefore by the reaction rate. The electrical potential in the solid is assumed to be constant in this model, because the solid has been taken as infinitely conductive to electrons. Thus, the overpotential will also be variable with position through the catalyst layer. The net ionic current density j_+[A cm^{-2}], which can also vary with position in the catalyst layer, is related to the electrical potential in the liquid electrolyte within the catalyst layer of the anode or the cathode, ϕ_L, by Ohm's law, shown in Equation 11:

Table 1. Summary of the model electrochemical parameters

	Anode	Cathode
Exchange current density/A cm^{-2}	10^{-8} at 150 °C	10^{-13} at 25 °C
Activation energy/kJ mol^{-1}	90	92
Transfer coefficient	1	1

$$j_+ = -k_E \frac{d\phi_L}{dz} \quad (11)$$

The effective acid conductivity, k_E, is a function of temperature, electrolyte concentration and the volume fraction of liquid in the catalyst layer.

The physical parameters contained in Equation 5 and 6 were determined by developing correlations from existing experimental data. Henry's law constant, K is related to the solubility:

$$K = RTc^* \quad (12)$$

where c^*, the solubility of propane in the liquid electrolyte, is linearly related to the partial pressure of propane in the gas filled pores. Experimental data [34] were used to obtain the following correlation for the variation of the oxygen solubility in phosphoric acid, c^* ([mol cm^{-3}]$_{LIQ}$ [Pa_{GAS}]$^{-1}$), with weight percent phosphoric acid concentration, W (%), for temperatures greater than 100 °C, which is normally the operating temperature range of PAFC's:

$$c* = 10^{-7}(6.87 - 0.062W) \quad (13)$$

A correlation relating the diffusivity of dissolved oxygen, D_{O_2}, in the electrolyte to the temperature, T, and the phosphoric acid concentration (weight percentage), W (%), was developed. Experimental data [35] for the diffusivity of oxygen in 98% phosphoric acid as a function of temperature were first fitted to an exponential correlation. The variation of oxygen diffusivity with phosphoric acid concentration was accounted for, using the Stokes–Einstein relation, which states that at the same temperature the diffusivity is inversely proportional to the solution viscosity. Data [36] for the viscosity of phosphoric acid solutions of different concentrations were used to obtain another correlation. The three relationships were then combined to obtain:

$$D_{O_2} = 0.048 \exp\left[-\frac{25770}{RT} + 0.034(98 - W)\right] \quad (14)$$

The solubility of propane in concentrated phosphoric acid is practically independent [2] of temperature and electrolyte concentration for temperatures greater than 100 °C in the concentration range 70–110 wt% H_3PO_4 used in this study. The solubility [2] is approximately 1.73 μmol cm^{-3} MPa^{-1}. The diffusivity of propane in the electrolyte has not been determined experimentally and so was estimated by means of the Wilke–Chang correlation [37]. According to the correlation, the diffusion coefficients for two different dissolved gases, D_1 and D_2, in the same solvent at a given temperature, are related to the molar volumes of the gases as:

$$\frac{D_1}{D_2} = \left(\frac{V_2}{V_1}\right)^{0.6} \tag{15}$$

On the basis of molar volumes of propane and oxygen ($V_{O_2} = 14.8$ cm^3 mol^{-1} ; $V_{C_3H_8} = 74.5$ cm^3 mol^{-1} [37]), their diffusivities in the same electrolyte are related by $D_p \approx 0.38\, D_{O_2}$, which was used to estimate the diffusivity of propane for different concentrations and temperatures using the value of D_{O_2} from Equation 14.

The effect of temperature on the equilibrium potential for the oxygen reduction reaction [37] is:

$$E_{EQ} = \frac{-4.184(-70650 - 8T\ln(T) + 92.84T)}{2F} \tag{16}$$

The equilibrium potential for the overall reaction at different temperatures has also been reported [2]. The equilibrium potential for the anodic reaction can be obtained by

$$E_{EQ} = E_{EQ,CAT} - E_{EQ,AN}. \tag{17}$$

At 25 °C, the equilibrium potential for the propane oxidation reaction is 0.139 V, and that for oxygen reduction is 1.229 V [2]. The effect of pressure on the equilibrium potential for the overall reaction is negligible and is not considered in the model. It was estimated [2] that for the range of temperatures considered in this model the equilibrium potential changes by 4 mV per 10-fold increase in pressure.

Values for the electrolyte properties were obtained from different sources. A correlation was developed to relate the conductivity of phosphoric acid electrolyte to the operating temperature and phosphoric acid concentration. It accounted for the effects of both porosity and tortuosity of the CL or ELL to which it was applied. Data for the water vapor pressure at different temperatures and electrolyte concentrations have been previously reported [36] and were used in this model. The activity of water for different molalities and for the concentration range of 50–85 wt% phosphoric acid, was obtained from a compilation [38]. The data have been fitted to the following correlations:

$$m = 0.371 \times e^{0.059W} \tag{18}$$

$$a_w = 0.870 \times e^{-0.039m} \tag{19}$$

The Stefan–Maxwell equations were used to describe gas diffusion in the gas diffusion layer and catalyst gas filled layer pores [39, 40]. As an example, the propane concentration profile in the catalyst layer is given by the following:

$$-\frac{dc_P^G}{dz} = \frac{c_{CO_2}N_P - c_P^G N_{CO_2}}{c_T D^E_{P,CO_2}} + \frac{c_w N_P}{c_T D^E_{P,W}} \tag{20}$$

where the molar fluxes are related by the reaction stoichiometry:

$$N_{CO_2} = -3N_P \tag{21}$$

The gas-phase propane flux in the catalyst layer varies according to the volumetric reaction rate:

$$\frac{dN_P}{dz} = R_V \tag{22}$$

where R_V was obtained from Equation 5. Equations analogous to Equation 20–22 have been used for the cathode electrode for the ternary system $O_2/N_2/H_2O$.

3. Computational method

The numerical methodology used to solve the above systems of equations and to obtain the fuel cell polarization curves is described here. The *iR*-drop from ionic transport through the electrolyte compartment of the fuel cell was computed at each selected current density j, using the integrated form of Equation 11 for constant current density.

$$\Delta\phi_{ELL} = (j/k_E)L_{ELL} \tag{23}$$

At any current density, the cell potential is related to the anode and cathode electrode potentials (E_{AN} and E_{CAT}) by

$$E_{CELL} = E_{CAT} - E_{AN} - \Delta\phi_{ELL} \tag{24}$$

The distributed *iR*-drop associated with ionic transport inside the electrodes was included in the E_{CAT} and E_{AN} terms in Equation 24.

The differential-algebraic system of equations for the anode electrode is summarized in Table 2. An analogous system of equations is valid for the cathode with C_3H_8, CO_2 and H_2O replaced by O_2, H_2O and N_2. The two systems were solved separately to obtain the anode and cathode potentials (E_{AN} and E_{CAT}) at each current density j. The procedure is similar for both the anode and the cathode. A diagram of the equations that were solved and the boundary conditions is shown in Figure 1. The functional relationship between the variables in the differential equations is shown inside each box. At the boundary between the gas diffusion layer and the catalyst layer, the concentrations and fluxes of the gases are required to be continuous. The output fluxes and concentrations at the right end of the gas diffusion layer (Figure 1) resulting from the solution of the gas-diffusion layer differential equations, are

Table 2. Summary of equations pertaining to the propane anode model

$\frac{dN_P}{dz} = R_V$ (Equation 22) $\quad \frac{dN_P}{dz} = 0$	Equation 22 A[a] (same in GDL)
$-\frac{dc_P^G}{dz} = \frac{c_{CO_2}N_P - c_P^G N_{CO_2}}{c_T D^E_{P/CO_2}} + \frac{c_w N_P}{c_T D^E_{P/W}}$	Equation 20 (same in GDL)
$-\frac{dc_{CO_2}}{dz} = \frac{c_P N_{CO_2} - c_{CO_2} N_P}{c_T D^E_{P/CO_2}} + \frac{c_w N_{CO_2}}{c_T D^E_{CO_2/W}}$	Equation 20 A[b] (same in GDL)
$c_T = c_P + c_{CO_2} + c_W$	Balance equation
$N_{CO_2} = -3N_P$	Equation 21
$R_V = \rho_{uAG} \frac{4\pi D^E D(r_{AG}+L_F)Kc_P^G a_w r_{AG}[r_{AG}\sqrt{\psi}\coth(r_{AG}\sqrt{\psi})-1]}{D(r_{AG}+L_F)+L_F D^E[r_{AG}\sqrt{\psi}\coth(r_{AG}\sqrt{\psi})-1]}$	Equation 5
$\psi = \left(\frac{S_A j_o}{nFc^{ss}D^E}\right)\exp\left(\frac{\alpha nF\eta}{RT}\right)$	Equation 6
$\eta = \phi_S - \phi_L - E_{EQ,AN}$	Equation 10
$\frac{d\phi_L}{dz} = \frac{j_+}{k_E}$	Equation 11
$\frac{dj_+}{dz} = 20FR_V$	Equation 22 B[c]

[a]Equation 22A is equivalent to Equation 22, except it is written for the GDL.
[b]Equation 20 A is equivalent to Equation 20, except it is written for the GDL.
[c]Equation 22B is Faraday's Law applied to Equation 22.

used as the input left-end boundary conditions for the catalyst layer equations. Two boundary conditions are specified at opposite ends of the electrode's CL: (a) the reactant gas molar flux is zero at the electrolyte-side of the CL because gas-filled pores terminate there, and (b) the ionic current in the electrolyte is zero at the boundary between the catalyst and the gas-diffusion layer, because liquid-filled pores terminate there. All other boundary conditions are satisfied naturally in the direction that the problem was solved, from left to right in Figure 1. Specifying two boundary conditions at the opposite sides of the catalyst layer caused a difficulty that was overcome using Newton's method. The boundary condition $N_{P2} = 0$ at the right end of the catalyst layer was satisfied as the target condition in an iterative routine. The input N_{P1}, at the left end of the gas diffusion layer, was used as the control variable that was adjusted by Newton's method to satisfy the target condition.

The solution procedure, for the anode electrode, can be described as follows: The partial pressure of the reactant gases was specified at the external surface of the

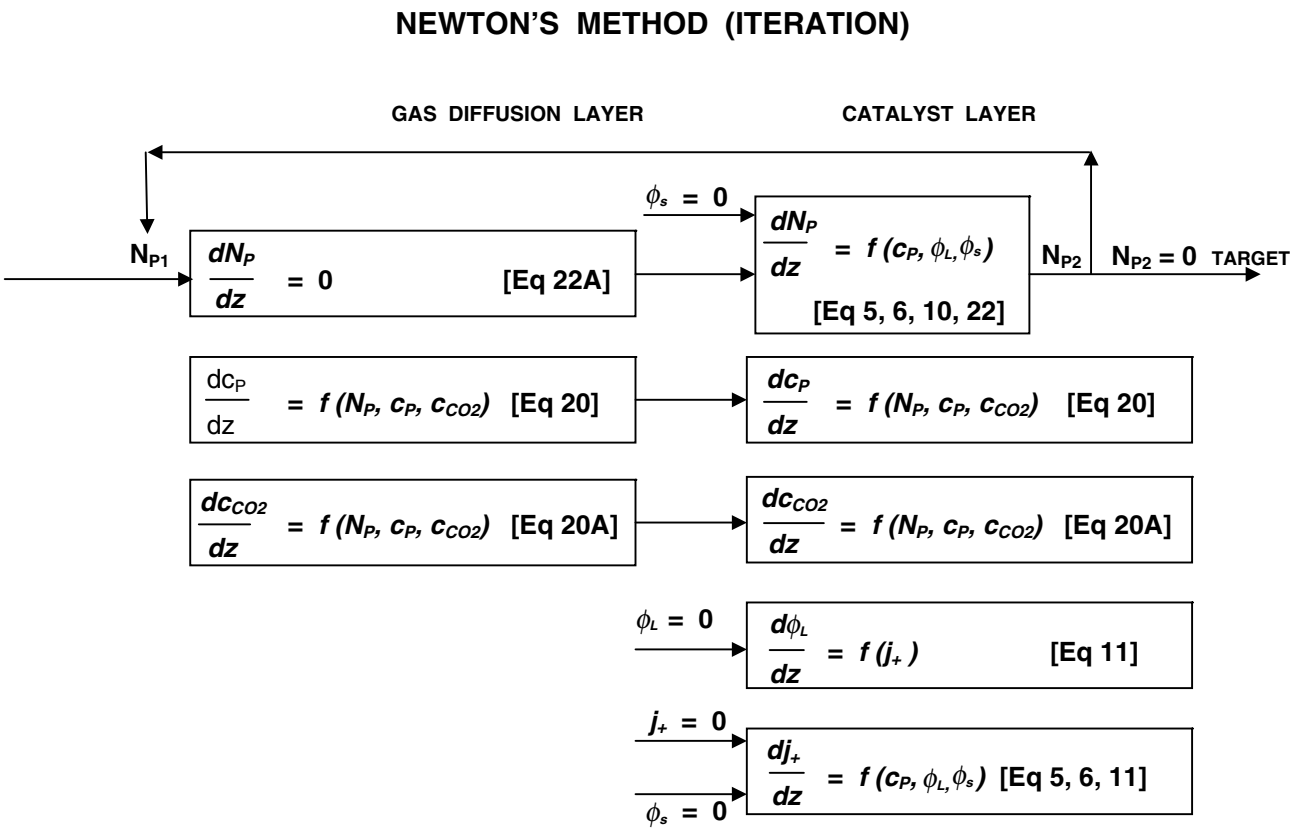

Fig. 1. Input/output diagram for both gas diffusion layer and catalyst layer domain equations indicating functional dependencies between variables and boundary conditions. Equations in parentheses appear in Table 2.

gas diffusion layer at the anode gas channel. This value was calculated from the total gas pressure and gas composition (corresponding to the local conversion) for the anode gas channel that was specified at the beginning of the simulation. The equations were solved by proceeding from the gas channel towards the electrolyte. Initially, the electrical potential in the anode solid phase Φ_S was specified starting from a small value near the anode equilibrium potential. Then the system of equations in the anode GDL and CL was solved iteratively and Newton's method was used to satisfy the boundary condition. In the beginning of the iterations, an initial guess for the propane molar flux from the anode GC at the external gas-supplying surface of the electrode (designated as N_{P1}) was specified and the program proceeded by solving the differential equations successively, Equation 20 for the GDL, and Equation 11, 20, and 22 for the catalyst layer. The volumetric reaction rate equation, Equation 22, gives rise to a variation in the propane molar flux through the CL. The required boundary condition at the electrode-electrolyte interface was $N_{P2} = 0$, where N_{P2} denotes the computed propane flux at the electrolyte side of the electrode. A minute perturbation, dN_{P1}, in flux ($dN_{P1} = 10^{-9} N_{P1}$) was made to the above guessed value of N_{P1} to obtain a new perturbed value of N_{P1}. The perturbed value of $N_{P1} = (N_{P1} + dN_{P1})$ was used to calculate a perturbed value for $N_{P2} = (N_{P2} + dN_{P2})$. By numerically computing the derivative dN_{P2}/dN_{P1} a new estimate for N_{P1} was obtained using Newton's iterative formula and used as an initial guess for the next iteration. The solution proceeded by determining such a subsequent estimate for N_{P1} after each iteration. This method resulted in satisfying the boundary condition $N_{P2} = 0$ to within the specified tolerance, that was taken to be $N_{P2} < 10^{-7} N_{P1}$. Within each iteration, the differential equations of the differential-algebraic equation system (Equations 11, 20 and 22) were solved by a standard Runge–Kutta routine. The code was written in MATLAB.

After convergence was achieved, the overall reaction rate was calculated, by numerically integrating the volumetric reaction rate over the thickness of the catalyst layer. It was converted to the current density using Faraday's law. The anode potential was calculated as the difference $E_{AN} = \phi_S - \phi_L$ at the electrolyte side of the electrode in order to correspond to the electrode potential that is experimentally measured. In this way, each point of the polarization curve was computed without specifying either the local current density or the overpotential as a starting point because both vary across the thickness of the catalyst layer. The calculation flow diagram is shown in Figure 2, which contains the solution procedure for the two electrodes as single boxes that correspond to Figure 1. The program then proceeded by increasing ϕ_S to a larger value and repeating the above calculation for a different point on the polarization curve. Increments of 0.01 V were used for the electrical potential, ϕ_S , in order to provide a sufficiently large number of points to simulate the polarization curve for the whole range of potentials. The same procedure was used for the cathode. Using the procedure described above, several closely-spaced points on the polarization curves (E_{AN} and E_{CAT} as a function of current density) were computed. In order to use Equation 24 to obtain the fuel cell polarization curve, it was necessary to compute E_{AN} and E_{CAT} at the same current densities j. This was done by interpolating the anode and cathode electrode potential curves to the same selected values of current densities j. Equation 24 was then used to obtain the cell potential as a function of produced current density. This is equivalent to subtracting the anode half-cell polarization curve from the cathode half-cell polarization curve and then

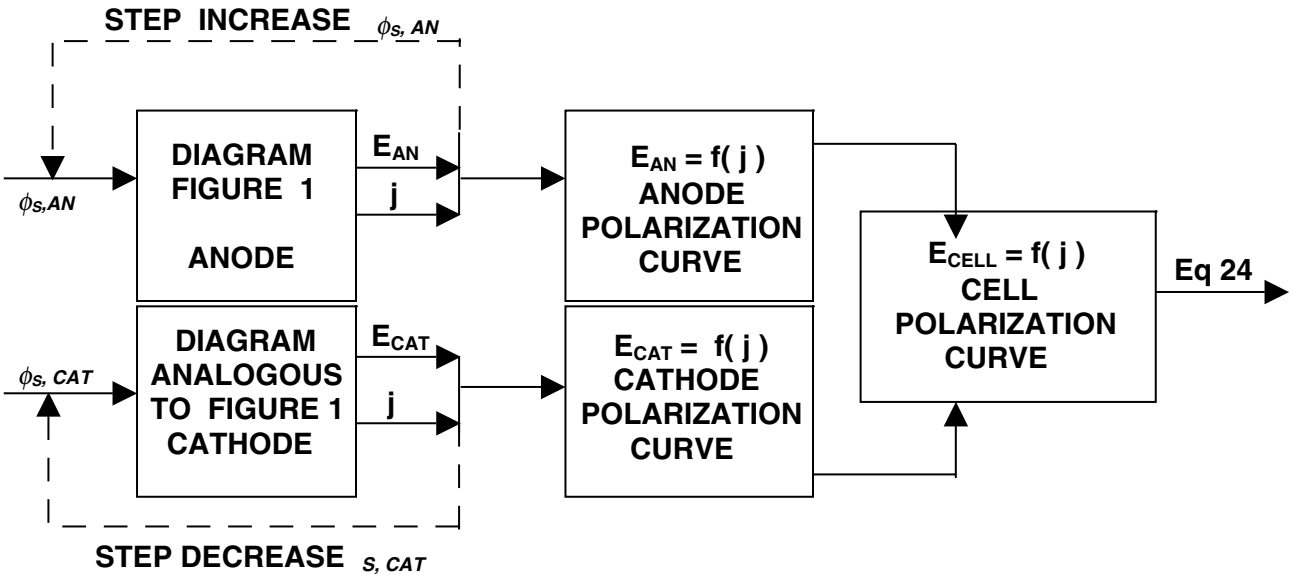

Fig. 2. Flow diagram of computational steps required to obtain the complete cell polarization curve.

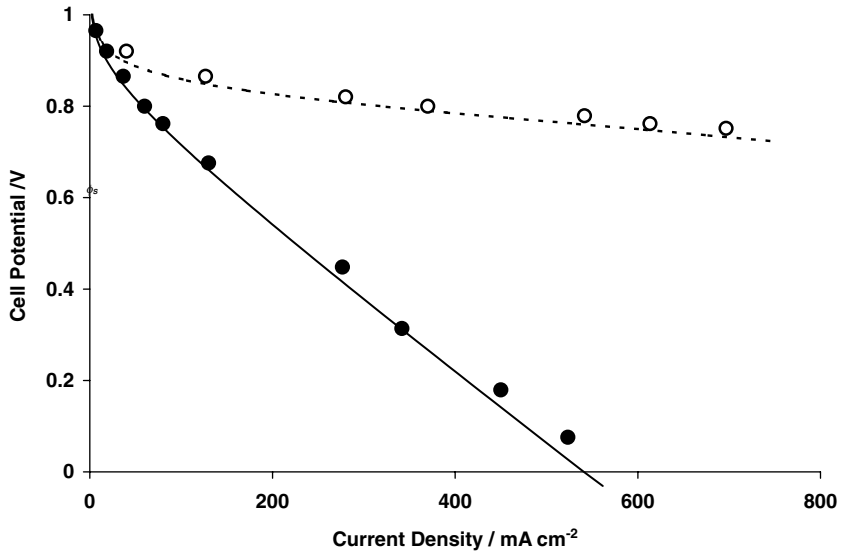

Fig. 3. Experimental data [17] and model results for H_2/O_2 cells. Platinum loading is 45 mg Pt cm^{-2} on cathode: ● experimental; —model; ○ experimental *iR*-free; - - -model *iR*-free.

subtracting the *iR*-drop in the electrolyte layer to obtain the cell potential curve.

4. Results and discussion

In order to validate the numerical model, its predictions were compared to experimental data [17] that was obtained with platinum black electrodes. These particular experimental data were selected for two reasons. First, several experimental variables were investigated so that it was possible to make comparisons at a variety of temperatures, reactant gas pressures, and phosphoric acid concentrations and thereby evaluate the capabilities of this numerical model. Second, the accompanying data [17, 18] included descriptions of the properties of the fuel cell materials (structure and geometrical properties; such as electrodes' thickness, electrolyte layer (spacer) thickness, catalyst layer thickness, gas diffusion layer thickness, Pt loading in the anode and the cathode, surface area of Pt per unit mass).

The particular electrodes used in the above studies [17, 18] were tested as cathodes and anodes for both H_2/O_2 fuel cells and C_3H_8/O_2 fuel cells. A comparison of their H_2/O_2 fuel cell experimental data (*iR*-included "solid circles" and the *iR*-free "open circles") and the polarization curve predictions of the numerical model in Figure 3 suggests that these electrodes are limited by the *iR*-drop caused by the relatively large thickness (0.32 cm) of the electrolyte layer (electrode thickness ~210 μm). Limiting current densities less than 600 mA cm^{-2} were observed. The agreement between

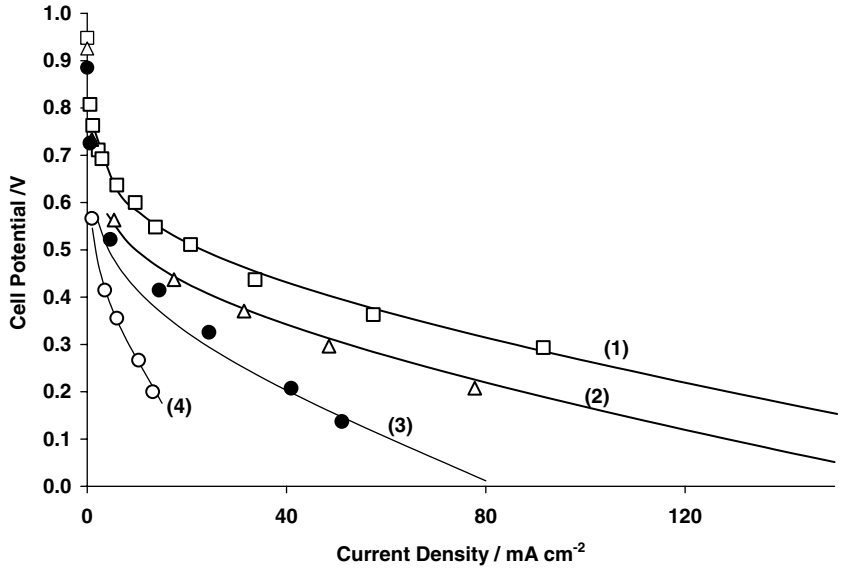

Fig. 4. Experimental data [17] and model predictions for C_3H_8/O_2 cells for different phosphoric acid concentration. The numbered solid lines denote model predictions. Platinum loading is 45 Pt mg cm^{-2} on each electrode. $T = 150$ °C. □, (1) 85% H_3PO_4; Δ, (2) 96% H_3PO_4; ●, (3) 101% H_3PO_4; ○, (4) 105% H_3PO_4.

the reported data (both the *iR*-included and the *iR*-free) and the polarization curves predicted by the mathematical model validate the model of a cathode (in H_2/O_2 fuel cells) having Pt black electrodes.

The propane/oxygen experimental fuel cell data [17] at 150 °C, obtained with the same unsupported Pt black electrodes at both anode and cathode, are compared with the corresponding model predictions in Figure 4, as a function of phosphoric acid concentration. The agreement is within 10% of the terminal fuel cell electrical potential for the entire range of current densities. There is a substantial decrease in performance as the concentration of H_3PO_4 increased. That decrease was predicted because the rate of the propane oxidation reaction in the model is proportional to the activity of water in solution. As the phosphoric acid concentration increases the corresponding decrease in concentration of free water molecules causes the reaction rate to decrease, since water is a reactant. The decrease was not related to other effects such as increased adsorption of a phosphoric acid species on Pt at large concentrations. This result is also consistent with the propane oxidation rate being first-order in water activity.

Experimental results at different combinations of temperature and electrolyte concentration, that together created a 80 kPa water vapor pressure above the electrolyte solution, are compared with model predictions in Figure 5. The effects of temperature and concentration in Figure 5 can be separated by referring to Figure 4, where performance decreased with increasing H_3PO_4 concentration at constant temperature. Figure 5 shows that the beneficial effect of increasing temperature more than offsets the negative effect of increasing H_3PO_4 concentration. The effect of *iR*-loss in Figure 5, seen by comparing lines (1) and (2), is consistent with its effect in Figure 3. The correspondence between the model predictions and the experimental data at the various combinations of temperature and phosphoric acid concentration, shown in Figure 5, is a further indication of the model's validity. Because the combination of 200 °C and 95 wt% H_3PO_4 was better than the other combinations shown in Figure 5, that combination was maintained while other variables were altered to determine their effect on fuel cell performance in Figures 6 to 8.

The agreement between the predictions made by the model and the experimental data demonstrated in Figures 3–5 suggests that the combination of equations and parameter values used in this model can accurately represent propane oxidation and oxygen reduction reactions on platinum catalysts in H_3PO_4 electrolytes, for the range of temperatures and acid concentrations included in this study. This success suggests that the model might be useful in predicting fuel cell performance at other conditions. The rest of this work concentrated on predicting the performance of C_3H_8/O_2 fuel cells, in which parameter values for supported Pt/C electrodes in modern hydrogen/oxygen PAFCs were used, instead of those for small surface-area, unsupported Pt black electrodes.

Further validation [21] of our model was obtained by comparing the predictions of our cathode-only model with experimental half-cell polarization curves obtained from two different cathode gas-diffusion electrodes representative of modern PAFCs that contain Pt catalyst supported on carbon. The comparison showed that the model can predict the cathode polarization curves for the whole range of current densities, including mass-transport limited conditions. Our cathode model contains a description of the following phenomena: surface processes on the catalyst (oxygen reduction), gas phase transport in gas-filled pores, dissolved gas transport in liquid-filled pores, and ionic transport. Both gas phase

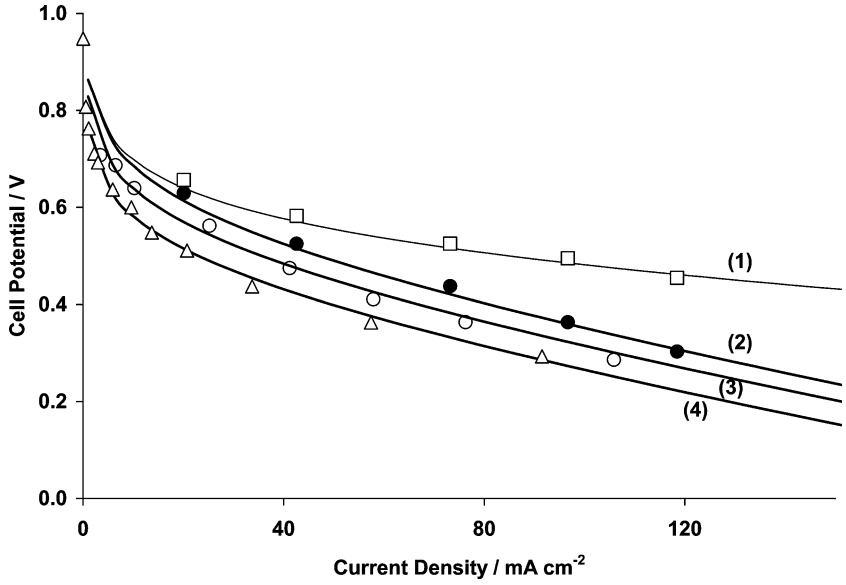

Fig. 5. Experimental data [17] and model predictions for C_3H_8/O_2 cells for different phosphoric acid concentration and temperature. The numbered solid lines denote model predictions. Platinum loading is 45 mg Pt cm^{-2} on each electrode. □, (1) 95% H_3PO_4, 200 °C, IR free; ●, (2) 95% H_3PO_4, 200 °C; ○, (3) 91% H_3PO_4, 175 °C; Δ, (4) 85% H_3PO_4, 150 °C.

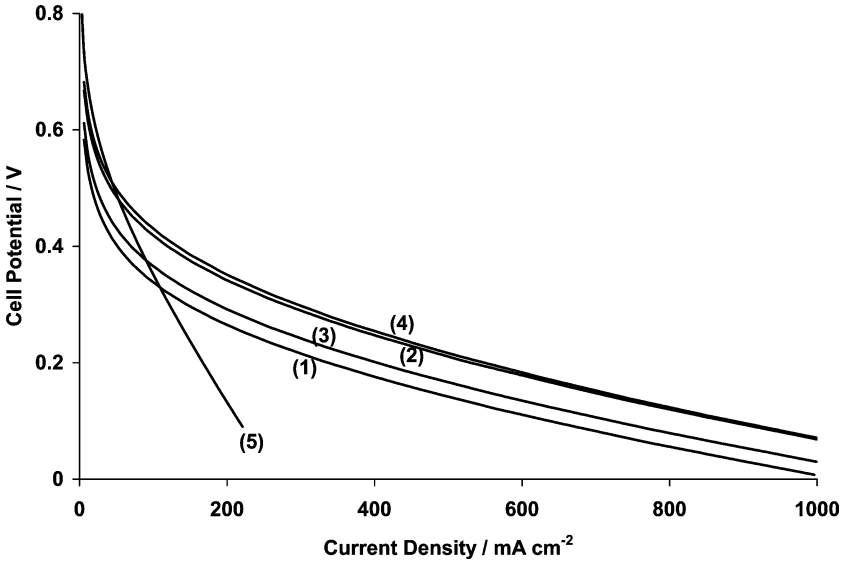

Fig. 6. Predicted performance curves for C_3H_8/O_2 cells for Pt/C electrodes, 200 °C, 95% H_3PO_4, 101.3 kPa, 20% utilization: (1–4) Electrode parameters given in Table 3; (5) Pt black electrodes [17] of 45 mg Pt cm^{-2} loading.

transport and dissolved gas transport processes in the propane anode are similar to those in the oxygen cathode. The difference is that the diffusing species are different. The ionic transport process also occurs in the catalysts layers of the cathode and the anode. Therefore, it can be argued that these processes have been described adequately, based on the validation of the cathode model with experimental cathode data. However, the processes for which we are less confident are the surface processes (adsorption, reaction, and surface diffusion rates) on the catalyst of the anode electrode. These processes should be very similar for both the supported Pt catalyst of modern PAFCs and the unsupported Pt catalyst of the electrodes described in Figures 3–5, since both have pure Pt as the electrocatalyst. Therefore, the same propane oxidation kinetic parameters were used for both the supported Pt on carbon electrocatalysts and the unsupported Pt electrocatalysts described in Figures 4 and 5.

On the basis of identical kinetic parameters, a comparison of the physical properties of unsupported platinum black electrodes with those of supported Pt electrodes suggests that the modern supported Pt electrodes may produce a substantially better performance. For example, it was reported [17, 18] that the platinum loading of the unsupported Pt black electrodes described in Figures 3–5 was 45 mg Pt cm^{-2}, the surface area per unit mass of Pt was 20 m^2 (g Pt)$^{-1}$, and the space between the electrodes had a thickness of ~0.32 cm. A smaller amount of platinum would be required if it was dispersed on a high surface area carbon support, > 120 m^2 (g Pt)$^{-1}$, which would require much less catalyst for analogous performance. Performance benefits should also be expected if a thinner

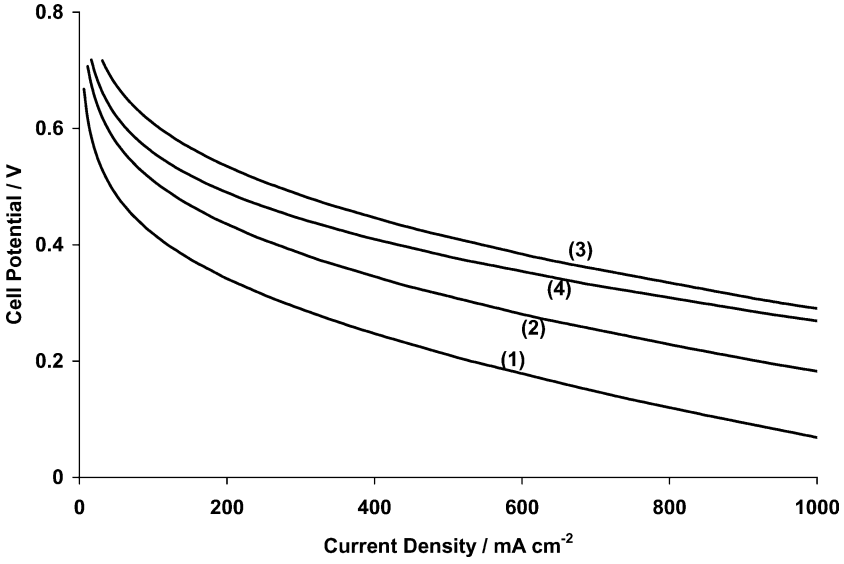

Fig. 7. Predicted effect of reactant gas pressure on performance of C_3H_8/O_2 cells, 200 °C, 95% H_3PO_4, 20% utilization: (1) 101.3 kPa, 5 mg Pt cm^{-2}; (2) 304 kPa, 5 mg Pt cm^{-2}; (3) 1013 kPa, 5 mg Pt cm^{-2}; (4) 1013 kPa, 2.5 mg Pt cm^{-2}.

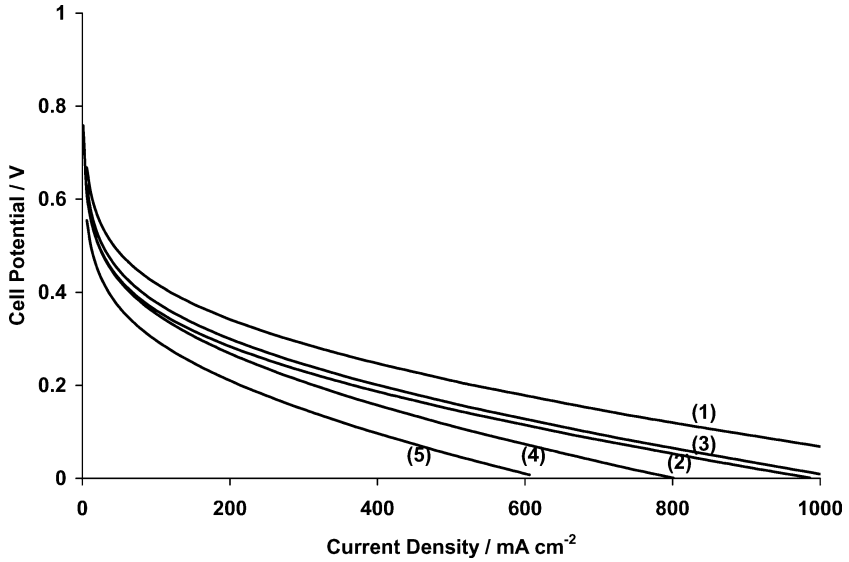

Fig. 8. Predicted effect of reactant gas local conversion on performance of C_3H_8/O_2 cells, 200 °C, 95% H_3PO_4, 101.3 kPa, 5 mg Pt cm^{-2}. Conversion with (1) 20%O_2, 20%C_3H_8; (2) 80%O_2, 20%C_3H_8; (3) 50%O_2, 50%C_3H_8; (4) 20%O_2, 80%C_3H_8; (5) 80%O_2, 80%C_3H_8.

electrolyte layer were used, thus decreasing the ohmic conduction losses.

Although the observation that supported catalysts are superior to unsupported ones for the oxidation of propane is valid for the particular electrodes used in Figures 4 and 5, it should not be generalized to all types of fuel cells. Recently Pt–Ru electrocatalysts were compared [41] in direct methanol fuel cells (DMFC), and it was found that unsupported Pt–Ru performed better than carbon-supported Pt–Ru. It was suggested that this might be caused by larger mass-transport losses for the supported catalysts because the supported catalysts contain catalyst sites in micropores that are not easily accessible. In addition, it was shown [41] that the Ru in the unsupported catalysts consisted of 50% RuO_2 and 50% Pt–Ru alloy, whereas the supported catalyst consisted entirely of the Pt–Ru alloy. A later study [42] concluded that the surface composition of Pt–Ru alloy nanoparticles has an important effect on electocatalyst performance. In our study of pure Pt catalysts, the surface chemical composition is the same for both supported and unsupported catalysts. Our model was based on the identical electrode surface composition and the same intrinsic kinetic parameters applying to both the pure Pt supported and the pure Pt unsupported catalysts. Finally, because both the microscopic structure of electrodes and operating conditions could differ in any two fuel cells, our conclusion about supported and unsupported catalysts is strictly valid only for the combination of electrodes and conditions examined here.

Figure 6 shows five predicted C_3H_8/O_2 polarization curves: one unsupported Pt black electrocatalyst and the four carbon supported platinum electrocatalysts, as listed in Table 3; for 95% H_3PO_4, atmospheric pressure, 200 °C, and 20% utilization of both propane and oxygen. For current densities greater than ~150 mA cm^{-2}, the predicted performance for the supported electrocatalyst with a total fuel cell loading of 2.5 mg Pt cm^{-2} (2 mg Pt cm^{-2} in the anode and 0.5 mg Pt cm^{-2} in the cathode) (line 1) is better than that for unsupported Pt black electrodes [17], that contained 90 mg Pt cm^{-2} total platinum loading (line 5). There are three explanations for the improved performance. The supported Pt/C electrodes: (1) have greater surface area per unit mass of Pt, (2) require less Pt when it is dispersed on a carbon support, and (3) have a lower *iR*-drop in the thinner SiC electrolyte matrix (250 μm thickness was assumed although they can be thinner [43]).

Doubling the amount of total Pt loading (lines 2, 3 and 4 compared to line 1 in Figure 6/Table 3) shows improved performance, as expected. However, there are at least two different ways to increase platinum loading. One way is to increase the electrode thickness and use the same Pt catalyst concentration (for example 10% Pt on C). In this case the larger ohmic and diffusion

Table 3. Electrode parameters corresponding to Figure 6 polarization curves

Line	Pt loading (mg Pt cm^{-2})			Catalyst layer thickness (μm)		Catalyst concentration (wt% Pt on C)	
	Cathode	Anode	Total	Cathode	Anode	Cathode	Anode
1	0.5	2	2.5	150	150	10%	40%
2	1	4	5	300	300	10%	40%
3	1	4	5	150	150	20%	80%
4	1	4	5	300	450	10%	26.7%

potential losses in the thicker electrode will offset part of the performance benefit that results from the increased amount of catalyst. The second way is to use the same electrode thickness and to increase the Pt catalyst concentration, i.e. to have a greater wt% of Pt metal in the Pt/C electrode. In the second case, increasing the amount of Pt on the same amount of carbon surface area, causes a decrease in the Pt surface area per unit mass of Pt available for reaction, and therefore decreases the dispersion of Pt particles, a phenomenon that becomes more pronounced as the catalyst concentration increases. A smaller dispersion of Pt offsets part of the performance benefit that results from the increased amount of catalyst. The predicted performance is much better when the Pt loading is increased by using thicker electrode catalyst layers (lines 2, 4) than by using greater concentrations of Pt on the carbon (line 3). This suggests that the increased ohmic and diffusion losses caused by thicker electrodes is not as detrimental as the smaller Pt dispersion. The model indicated that the combination shown in line 4, corresponding to the smallest weight % of Pt in the Pt/C electrode, had the best performance among the electrodes that contained 5 mg Pt cm^{-2}.

The effect of reactant gas pressure is predicted in Figure 7, for equal gas pressures in the anode and cathode gas channels of the fuel cell. For lines 1–3, the other parameters were fixed to those of Figure 6, line 2. For 1013 kPa pressure (line 3) and a current density of $\sim$1 A cm^{-2}, a cell potential of 0.3 V was predicted with a 5 mg Pt cm^{-2} total platinum loading. The performance predicted for 2.5 mg Pt cm^{-2} (line 4) is only slightly worse. These predictions suggest that operation at high pressure may be particularly beneficial for direct hydrocarbon fuel cells.

The effects of propane and oxygen conversions were predicted in Figure 8. The results correspond to a local conversion at a specific location along the anode and cathode gas channels. For example, 5% propane conversion would correspond to a location in the anode gas channel that is close to the gas channel inlet, while larger values of propane conversion would correspond to locations further from the inlet. The relative local conversion of oxygen and propane can be independently controlled by adjusting the gas flowrates in the gas-supplying channels or by changing the relative positions of inlet gas manifolds (co-current or counter-current flow). Thus, it is possible to have high oxygen conversion locations corresponding to small fuel conversion locations in counter-current flow of the fuel and oxidant in the gas channels, or the reverse, so that several cases were considered. The results show that the performance deteriorates at large propane and oxygen conversions and the effect of propane conversion is more significant than oxygen conversion.

The effect of the operating temperature, for operation at high pressure (1013 kPa), is shown in Figure 9. Operation at high pressure allows larger vapor pressures and therefore greater temperatures. It is predicted that increasing the temperature to 215 °C (line 3) causes an improved performance. A further increase in temperature, allowed by using a more concentrated electrolyte, will not necessarily improve performance (line 4). This is because the opposing effect of increasing the acid concentration becomes controlling when very little water is available for reaction.

The predicted performances of two propane fuel cells, one operating with an air cathode and one operating with an oxygen cathode, are shown in Figure 10. The additional potential loss, that is observed when the cathode feed is air rather than oxygen, is caused by the lower oxygen reactant concentration in the cathode electrode pores. This decreases the driving force for the oxygen reduction reaction because the reaction rate depends on the oxygen concentration. This difference in performance is strictly associated with the cathode

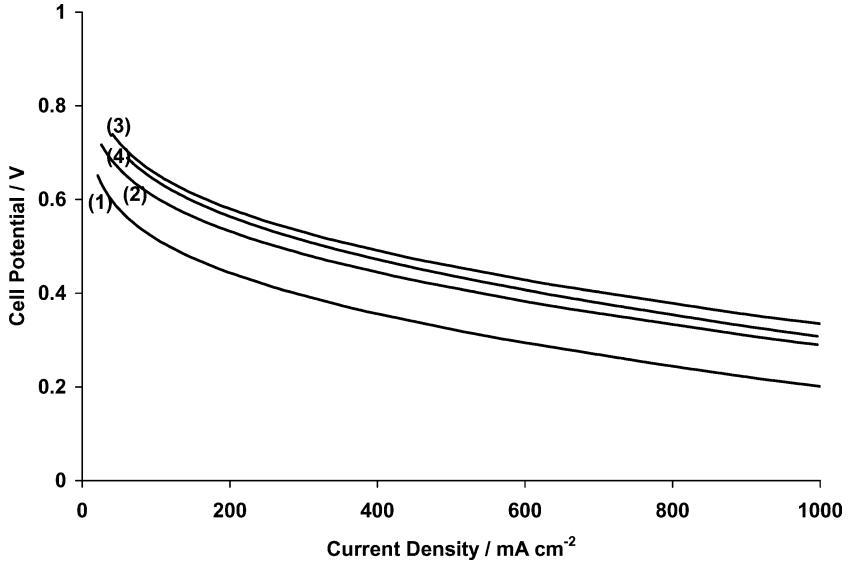

Fig. 9. Predicted effect of operating temperature on the performance of C_3H_8/O_2 cells for Pt/C electrodes, 1013 kPa, 5 mg Pt cm^{-2}: (1) 185 °C, 95%H_3PO_4; (2) 200 °C, 95% H_3PO_4; (3) 215 °C, 95% H_3PO_4; (4) 230 °C, 100% H_3PO_4.

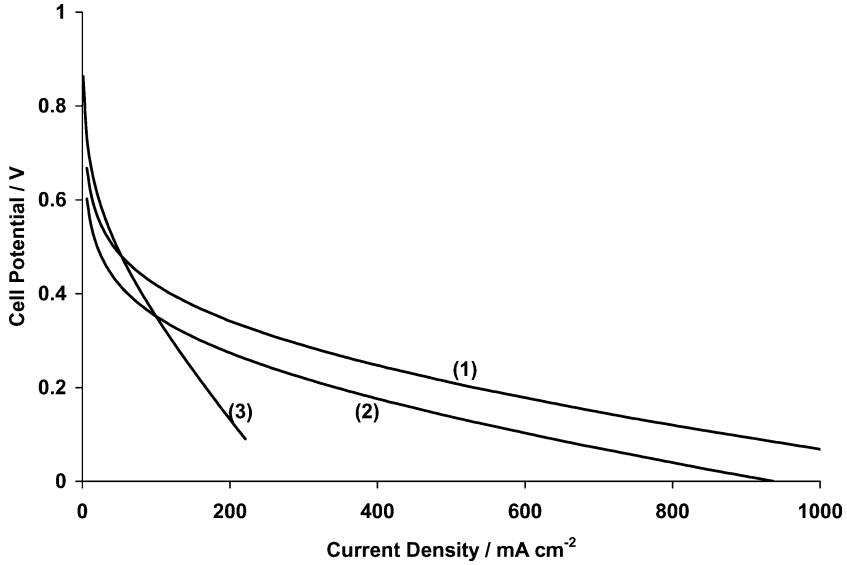

Fig. 10. Predicted performance curves for C_3H_8 cells with Pt/C electrodes for oxygen cathode (line 1) and air cathode (line 2); 200 °C, 95% H_3PO_4, 101.3 kPa, 20% utilization, 5 mg Pt cm^{-2}. Pt black (line 3) polarization curve [17] (90 mg Pt cm^{-2}) is shown for comparison.

electrode. Compared to air, the improved performance of operation with pure oxygen is offset by its greater cost. Figure 10 would be useful in quantifying the differences in performance when selecting a cathode feedstock. The line corresponding to the previously examined Pt – black electrodes is also shown for comparison.

In summary, polarization curves were predicted for direct propane fuel cells with Pt/C electrodes of varying Pt loading and operating conditions. This model predicts a maximum power density of 100 mW cm^{-2}, for a propane/oxygen cell utilizing Pt/C electrodes and 95% phosphoric acid electrolyte at 200 °C, 101.3 kPa propane gas pressure, 101.3 kPa oxygen gas pressure, 4 mg Pt cm^{-2} loading of platinum in the anode and 1 mg Pt cm^{-2} loading of platinum in the cathode. It is interesting to note that the maximum power density obtained [16] for a direct propane fuel cell utilizing a membrane electrolyte, with Pt–CrO_3 anode catalyst supported on carbon and total platinum loading of 2.4 mg Pt cm^{-2}, operating at 95 °C, showed a maximum power density of 46 mW cm^{-2}. Although different systems (membrane electrolyte vs H_3PO_4 electrolyte) and temperatures (95 vs 200 °C) were used, this comparison suggests that results predicted by the model are of the same order of magnitude as recent experimental results obtained with modern electrodes.

Figure 11 indicates the predicted polarization (electrical potential loss) for three different electrodes: a propane anode containing 4 mg Pt cm^{-2} an oxygen

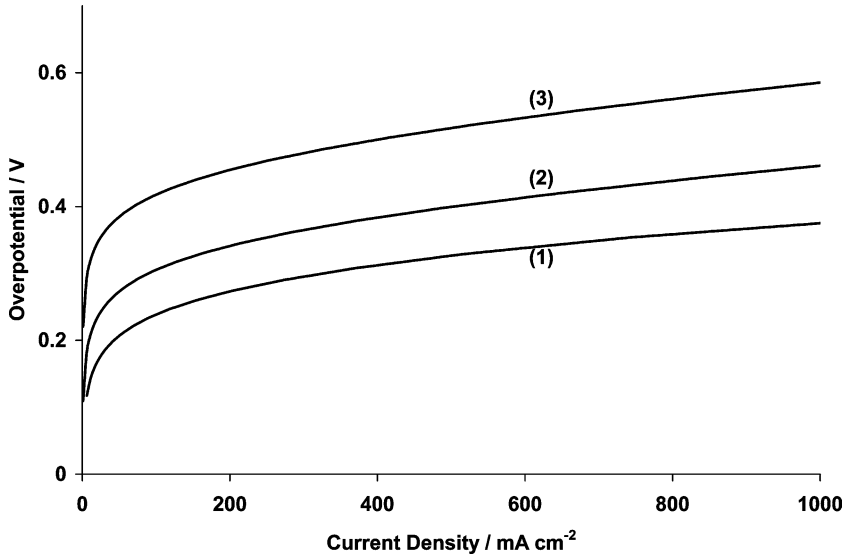

Fig. 11. Predicted electrode potential loss at 200 °C, 101.3 kPa for an oxygen cathode (line 1) containing 1 mg Pt cm^{-2}, an air cathode (line 2) containing 1 mg Pt cm^{-2} and a propane anode (line 3) with 4 mg Pt cm^{-2}.

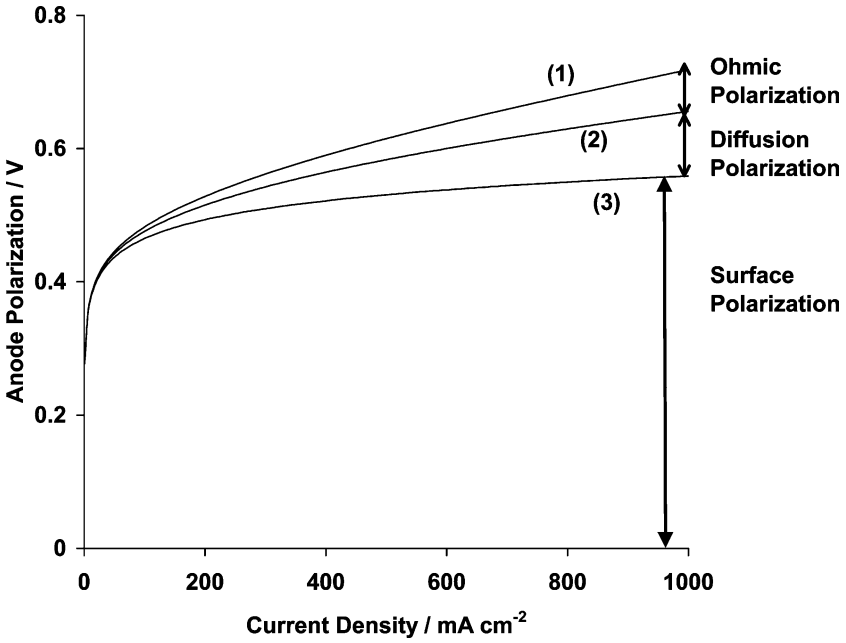

Fig. 12. Predicted polarization curve for a propane anode (200 °C, 101.3 kPa, 4 mg Pt cm^{-2}) after successive elimination of various resistances at 80% local propane conversion: (1) all resistances included; (2) no ionic conduction loss; (3) no diffusion loss in agglomerates, liquid film or gas phase.

cathode containing 1 mg Pt cm^{-2} and an air cathode containing 1 mg Pt cm^{-2} . The electrical potential loss for the propane electrode is much greater than that for the oxygen or air cathodes. This also suggests that in order to achieve better performance in a DHFC, the greatest proportion of the total Pt loading should be allocated to the anode.

The various resistances that cause potential losses in a propane anode electrode were also examined. They are activation polarization (caused by surface processes), concentration polarization (caused by the various diffusion processes), and ohmic polarization (caused by ionic transport). Figure 12 shows the electrode polarization (electrical potential loss) vs the current-density curves after subsequently eliminating each resistance. The elimination of each resistance was done by forcing the relevant parameters to extremely high values (10^{10}). For example, to eliminate the ohmic overpotential, the electrolyte ionic conductivity was given an extremely large number. Figure 12 shows that for all current densities considered the process that overwhelmingly determines the anode polarization is the electrochemical reaction on the surface of the anode catalyst. This result is very important because it suggests that any significant improvement of the direct propane fuel cell anode can only be achieved if the rate of the catalyst surface processes (adsorption, desorption, charge transfer reaction) is increased. The curves in Figure 12 show that gas diffusion and ionic transport processes have only a minor effect. The results also suggest that the effect of uncertainties in physicochemical variables not directly related to the surface reaction (such as propane diffusion coefficient in the gas and liquid phase and the electrolyte conductivity) can be considered to be insignificant.

5. Conclusions

Five conclusions can be drawn from the work described here. First, the numerical model was shown to accurately represent (predicted potentials normally within ± 0.02 V at any current density) existing experimental data (polarization curves) for direct propane fuel cells having phosphoric acid electrolytes and unsupported platinum black electrodes. Second, the inclusion of the activity of water in the description of the propane oxidation reaction explained the strong dependence of fuel cell performance on electrolyte concentration. Third, the anode over-potential was shown to be larger than that of the cathode, regardless of whether air or oxygen was used at the cathode. A significant improvement in DHFC performance would be achieved by decreasing the electrical potential losses caused by surface phenomena on the anode catalyst. Fourth, for a constant amount of platinum, [mg Pt per cm^2 of electrode face area], the numerical predictions indicated that thicker electrodes with smaller Pt/C ratios are superior to thinner electrodes with larger Pt/C ratios for the ranges of platinum loading and catalyst layer thicknesses evaluated here. Fifth, the model compared DHFC performance of unsupported platinum black electrodes to modern electrodes having the platinum dispersed on a carbon support and showed that for equal kinetic parameters the modern electrodes were substantially superior. Finally, in our opinion future research leading to improved electrocatalyst performance will lead to a substantial overall improvement in DHFC performance. Some of our current modeling efforts are focused on a detailed mathematical description of the reaction steps that occur on the surfaces of anode electrocatalysts.

Acknowledgements

Financial assistance from the Natural Sciences and Engineering Research Council of Canada for the support of one of the authors, George Psofogiannakis, is greatly appreciated.

References

1. H.A. Liebhafsky and E.J. Cairns, *Fuel Cells and Fuel Batteries* (Wiley, New York, 1968), p. 458.
2. J.O'M. Bockris and S. Srinivasan, *Fuel Cells: Their Electrochemistry* (McGraw-Hill, New York, 1969), p. 357.
3. E.J. Cairns, *in*: P. Delahay and C.W. Tobias (Eds), *Advances in Electrochemistry and Electrochemical Engineering*, Vol.8 (Wiley, New York, 1971), 337 pp.
4. E.J. Cairns and D.I. Macdonald, *J. Electrochem. Technol.* **2** (1964) 65.
5. E.J. Cairns and E.J. McInerney, *J. Electrochem. Soc.* **114** (1967) 980.
6. E.J. Cairns, *J. Electrochem. Soc.* **113** (1966) 1200.
7. E.J. Cairns, A.M. Breitenstein and A.J. Scarpellino, *J. Electrochem. Soc.* **115** (1968) 569.
8. J.W. Johnson, H. Wroblowa and J.O'M. Bockris, *J. Electrochem. Soc.* **111** (1964) 863.
9. J.O'M. Bockris, E. Gileadi and G.E Stoner, *J. Phys. Chem.* **73** (1969) 427.
10. R.V. Marvet and O.A Petrii, *Elektrokhimiya* **3** (1967) 153 (in Russian); 127 (English translation).
11. J.W. Johnson, S.C. Lai and W.J. James, *Electrochim. Acta* **15** (1970) 1511.
12. S.Y. Hsieh and K.M. Chen, *J. Electrochem. Soc.* **124** (1977) 1171.
13. V.S. Bagotzky, Yu.B. Vassiliev and O.A. Khazova, *J. Electroanal. Chem.* **81** (1977) 229.
14. M.G. Sustersic, R. Cordova, W.E. Triaca and A.J. Arvia, *J. Electrochem. Soc.* **127** (1980) 1242.
15. F. Hahn and C.A. Melendres, *Electrochim. Acta* **46** (2001) 3525.
16. O. Savadogo and F.J.R. Varela, *J. New Mater. Electrochem. Sys.* **4** (2001) 93.
17. W.T. Grubb and C.J. Michalske, *J. Electrochem. Soc.* **111** (1964) 1015.
18. J.H. Hirschenhofer, D.B Stauffer, R.R Engleman and M.G Klett, *Fuel Cell Handbook*, 4th ed., DOE/FETC-99/1076 (National Technical Information Service, U.S. Department of Commerce, Springfield, VA, 1998) 257 pp.
19. L.W. Niedrach and H.R. Alford, *J. Electrochem. Soc.* **112**(2) (1965) 117.
20. M.L. Perry, J. Newman and E.J. Cairns, *J. Electrochem. Soc.* **145** (1998) 5.
21. G. Psofogiannakis, A Mathematical Model for a Propane Phosphoric Acid Fuel Cell, Dissertation (University of Ottawa, Ottawa, Ontario, Canada, 2003).
22. J. Giner and C. Hunter, *J. Electrochem. Soc.* **116** (1969) 1124.
23. M.B. Cutlip, *Electrochim. Acta* **20** (1975) 767.
24. G. Maggio, *J. Appl. Electrochem.* **29** (1999) 171.
25. H.R. Kunz and G.A. Gruver, *J. Electrochem. Soc.* **122** (1975) 1279.
26. R.P. Iczkowski and M.B. Cutlip, *J. Electrochem. Soc.* **127** (1980) 1433.
27. P. Björnbom, *Electrochim. Acta* **32** (1987) 115.
28. S.C. Yang, M.B. Cutlip and P. Stonehart, *Electrochim. Acta* **34** (1989) 703.
29. S.C. Yang, *J. Electrochem. Soc.* **147** (2000) 71.
30. S.R. Choudhury, M.B. Deshmukh and R. Rengaswamy, *J. Power Sources* **112** (2002) 137.
31. A.J. Appleby, *in*: B.E.Conway and J.O'M. Bockris (Eds), *Modern Aspects of Electrochemistry*, Vol. 9 (Plenum Press, New York, 1974) 369 pp.
32. A.J. Appleby, *J. Electrochem. Soc.* **117** (1970) 328.
33. H.R. Kunz and G.A. Gruver, *Electrochim. Acta* **23** (1978) 219.
34. K.E. Gubbins and R.D. Walker Jr., *J. Electrochem. Soc.* **112** (1965) 469.
35. B.R. Scharifker, P. Zelenay and J.O'M. Bockris, *J. Electrochem. Soc.* **134** (1987) 2714.
36. D.R Gard, *in*: J.I. Kroschwitz and M. Howe-Grant (Eds), *Kirk Othmer Encyclopedia of Chemical Technology*, 4th ed., Vol.18 (Wiley, New York 1991) 669 pp.
37. R.C Reid, J.M. Prausnitz and T.K Sherwood, *The Properties of Gases and Liquids*, 3rd ed. (McGraw Hill, New York, 1977) pp. 567; 37a, ibid 58 pp.
38. A.J. Gordon and R.A. Ford, *The Chemist's Companion: A Handbook of Practical Data, Techniques and References* (Wiley, New York, 1970), p. 537.
39. R.B. Bird, W.E. Stewart and E.N. Lightfoot, *Transport Phenomena*, 1st ed., (Wiley, New York, 1960), p. 570.
40. L.B. Rothfeld, *A.I.Ch.E. J.* **9** (1963) 19.
41. A.S. Arico, A.K. Shukla, K.M. El-Khatib, P. Creti and V. Antanucci, *J. Appl. Electrochem.* **29** (1999) 671.
42. D. Cao and S.H. Bergens, *J. Power Sources* **134** (2004) 170.
43. M.I. Caires, M.L. Buzzo, E.A. Ticianelli and E.R. Gonzalez, *J. Appl. Electrochem.* **27** (1997) 19.